Acta Crystallographica Section D
Biological Crystallography
ISSN 0907-4449

Packing and loop-structure variations in non-isomorphous crystals of FabZ from *Plasmodium falciparum*

Pidugu Lakshmi Swarnamukhi,[a] Shailendra Kumar Sharma,[a] Prasanth Padala,[a] Namita Surolia,[b] Avadhesha Surolia[a,c] and Kaza Suguna[a]*

[a]Molecular Biophysics Unit, Indian Institute of Science, Bangalore 560012, India, [b]Molecular Biology and Genetics Unit, Jawaharlal Nehru Centre for Advanced Scientific Research, Bangalore 560064, India, and [c]National Institute of Immunology, New Delhi 110067, India

Correspondence e-mail: suguna@mbu.iisc.ernet.in

Received 22 November 2006
Accepted 20 January 2007

PDB References: PfFabZ, form 2, 2oki, r2okisf; form 3, 2okh, r2okhsf.

The crystals obtained from various batches of crystallization trials of FabZ from *Plasmodium falciparum* exhibited non-isomorphism. The *c* axis of the *I*222 cell showed a large variation of about 16 Å, from $c = 81$ Å to $c = 97$ Å. Complete data sets were collected for three crystal forms with varying lengths of the *c* axis (form 1, $c = 97$ Å; form 2, $c = 92$ Å; form 3, $c = 81$ Å). The crystal structure of form 1 has been reported previously. Here, the crystal structures of the other two crystal forms are reported and a detailed structural comparison is made of the three crystal forms in order to explore the possible reasons for the existence of non-isomorphism. The conformations of three loops vary between the three crystal forms. The disposition of the loops affects the crystal packing and hence the unit-cell parameter. The crystallization condition and crystallization method employed, which change the evaporation rate, determine the crystal form of the enzyme. The present analysis shows that pH-induced intrinsic conformational changes in the protein play a key role in the observed differences.

1. Introduction

Polymorphism is a commonly observed phenomenon in biological macromolecules, as the behaviour of macromolecules in crystallization experiments is quite unpredictable. Crystals with different unit-cell parameters or lattices are sometimes observed in the same crystallization drop. In addition, non-isomorphism in protein crystals arising during heavy-atom derivatization and cryocooling is quite common and is a serious problem in structure solution. Although the presence of non-isomorphism has been reported in many cases (Redinbo *et al.*, 1999; Verschueren *et al.*, 1999; Randal & Kossiakoff, 2000; Brodersen *et al.*, 2003), the possible structural reasons for the origination of non-isomorphism have not been explored, except in a few cases such as the cofactor-binding fragment of CysB (Verschueren *et al.*, 1999) and human topoisomerase I (Redinbo *et al.*, 1999). Recently, Dauter *et al.* (2005) reported orientation differences in the arrangement of Lon protease molecules in nearly isomorphous crystals of wild-type and mutant enzyme and showed that isometry of the unit cell is not necessarily an indication of true isomorphism. Analysis of the origin of non-isomorphism can only be carried out after structure solution. An understanding of this phenomenon might help in exploring new techniques to overcome this serious problem in structure solution.

In living systems, fatty acids, which are essential components of phospholipids and sphingolipids, are synthesized by two distinct pathways. In fungi, mammals and some mycobacteria, fatty acids are synthesized *via* an associative pathway

(type I FAS), in which a distinct domain of a single multi-domain protein catalyzes each reaction. In contrast, plants and most bacteria synthesize fatty acids by a different mechanism known as the type II or dissociative fatty-acid synthesis pathway (type II FAS; Raetz, 1990), in which each reaction is catalysed by a distinct enzyme and the intermediates are shuttled from one enzyme to another by a small acyl carrier protein (ACP; Rock & Cronan, 1996). β-Hydroxyacyl-ACP dehydratase (FabZ) catalyzes the third step in fatty-acid elongation in type II FAS, *i.e.* the dehydration of β-hydroxy-acyl-ACP to *trans*-2-enoyl-ACP (Brock *et al.*, 1967; Heath & Rock, 1996).

We have recently reported the crystal structure of FabZ from the malaria parasite *Plasmodium falciparum* (PfFabZ) as a dimer (d-PfFabZ) at low pH (Swarnamukhi *et al.*, 2006). As reported previously, d-PfFabZ was crystallized using hanging-drop vapour-diffusion and microbatch methods (Mukhi *et al.*, 2004). During the optimization of the crystallization conditions, highly non-isomorphous crystals were obtained. The *c* axis of the *I*222 cell varies significantly, whilst the *a* and *b* axes remain nearly the same. Small variation in any crystallization parameter leads to large differences in the *c* axis. Here, we report the crystal structure of d-PfFabZ in two new crystal forms with significant differences in one of the unit-cell parameters and compare them with the previously reported crystal structure of d-PfFabZ (form 1; c = 97 Å). Analysis of crystal packing shows that conformational changes induced at low pH play a major role in this non-isomorphism. Variations in crystallization parameters also exert an influence on the observed non-isomorphism.

Table 1
Data-collection and refinement statistics.

Values in parentheses are for the highest resolution shell.

	Form 1†	Form 2	Form 3
Data collection			
Resolution (Å)	31.0–2.4 (2.53–2.40)	30.0–2.7 (2.81–2.70)	30.0–3.0 (3.11–3.0)
Space group	*I*222	*I*222	*I*222
Unit-cell parameters (Å)			
a (Å)	71.5	72.0	70.0
b (Å)	82.6	81.9	81.5
c (Å)	96.5	91.6	80.8
Unit-cell volume (Å^3)	569922	533417	460700
Matthews coefficient (Å^3 Da^{-1})	2.2	2.0	1.7
Solvent content (%)	45	38	27
Temperature (K)	100	100	100
Total No. of reflections	71895	38712	18416
Unique reflections	11456 (1641)	8316 (827)	4840 (476)
$R_{\rm merge}$ (%)	7.5 (41.8)	5.6 (29.0)	8.5 (30.0)
Completeness (%)	100.0 (100.0)	96.4 (90.0)	98.0 (92.4)
$I/\sigma(I)$	20.7 (4.1)	21.5 (4.6)	14.5 (3.31)
Refinement			
Resolution range (Å)	31.0–2.4	30.0–2.7	30.0–3.0
No. of reflections	11435	8267	4835
No. of atoms			
Protein	2030	1845	1841
Water	95	15	20
R factor (%)	22.1	25.8	24.2
$R_{\rm free}$ (%)	24.7	28.6	29.1
Average *B* factor (Å^2)	44.8	60.3	67.6
R.m.s. deviations			
Bond lengths (Å)	0.007	0.010	0.010
Bond angles (°)	1.70	1.64	1.83
Dihedral angles (°)	26.6	25.8	30.2
Residues in Ramachandran plot (%)			
Most favoured region	85.0	80.0	80.2
Allowed region	13.6	18.5	17.8
Generously allowed region	1.4	1.5	2.0

† The statistics for form 1 have been reported previously (Swarnamukhi *et al.*, 2006) and are tabulated here for comparison.

2. Materials and methods

PfFabZ (Ile87–Lys230) was cloned and purified as reported previously (Sharma *et al.*, 2003). The purification protocol is essentially the same as in the previous work (Sharma *et al.*, 2003), except that the secondary culture was induced with 0.6 m*M* isopropyl β-D-thiogalactopyranoside (IPTG) and 10% glycerol was added to all the buffers during purification steps, which enhanced the protein yield and stability considerably.

Crystallization of purified PfFabZ was carried out at room temperature using the hanging-drop vapour-diffusion method by mixing 2 µl of approximately 10 mg ml^{-1} protein with 2 µl well solution. d-PfFabZ crystals were obtained in the range pH 4–5 with 20–30% PEG 4000 as the precipitant in 0.1 *M* acetate buffer and 0.2 *M* sodium acetate, as reported previously (Mukhi *et al.*, 2004). Further optimization was carried out by varying the protein-to-precipitant volume ratio (1:1, 1:2, 2:1, 2:3, 3:1, 3:2) in the drop, varying the volume of the reservoir solution (300–1000 µl), including additives and replacing sodium acetate with various monovalent and divalent acetates. Crystals of d-PfFabZ were obtained in the presence of various acetates, *i.e.* 0.2 *M* sodium acetate, ammonium acetate, potassium acetate, lithium acetate and magnesium acetate. The microbatch method was also employed for all the above conditions using a 72-well Terasaki plate from Greiner and silicone oil from Sigma–Aldrich. Crystals appeared in 2–3 d and reached maximum dimensions within a week. The crystals with the best diffraction quality were obtained using the microbatch method with ammonium acetate as the precipitant (Mukhi *et al.*, 2004).

X-ray diffraction data were collected using a MAR345 imaging plate. The X-ray beam (Cu $K\alpha$ radiation) from a Rigaku Ultrax-18 rotating-anode X-ray generator operating at 50 kV and 80 mA was focused with an Osmic mirror system. Crystals of d-PfFabZ were soaked in mother liquor containing 20% glycerol for 5 min and immediately flash-cooled using a liquid-nitrogen stream. The data sets were processed with *DENZO* and *SCALEPACK* (Otwinowski & Minor, 1997). Many crystals of d-PfFabZ from various crystallization trials were tested for diffraction. All the crystals belonged to space group *I*222, but they showed a large variation in the *c* axis. Of the various crystals that were checked, three crystal forms with c = 97 Å (form 1), c = 91 Å (form 2) and c = 81 Å (form 3) occurred most frequently. Complete data sets were collected to 2.7 and 3.0 Å resolution, respectively, for form 2 (c = 91 Å) and form 3 (c = 81 Å) crystals under cryoconditions (100 K). Details of data collection and processing are given in Table 1. The values of the Matthews coefficient are 2.0 and 1.7 Å^3 Da^{-1} and the solvent contents are 38 and 27%,

respectively, for form 2 and form 3 crystals, assuming the presence of a dimer in the asymmetric unit. The structure was solved by the molecular-replacement method using the program *Phaser* (Storoni *et al.*, 2004) with the crystal structure of d-PfFabZ (form 1; PDB code 1zhg) as a search model. Refinement was carried out using *CNS* (Brünger *et al.*, 1998) and the model was built by visual inspection using the graphics program *Coot* (Emsley & Cowtan, 2004). 5% of the observed reflections were reserved for the calculation of $R_{\rm free}$. *PROCHECK* (Laskowski *et al.*, 1993) was used to validate the stereochemical quality of the final models. Structural superpositions were carried out using the program *ALIGN* (Cohen, 1997). The atomic interactions were calculated using the program *CONTACT* from the *CCP*4 program suite (Collaborative Computational Project, Number 4 1994).

3. Results and discussion

3.1. Crystallization of d-PfFabZ

During the optimization of the crystallization conditions, non-isomorphous crystals were obtained. All the crystals belong to the same space group *I*222, but differ in the length of their *c* axes. From Table 2, it is apparent that the length of the *c* axis is dependent on the method of crystallization adopted and hence on the differences in the evaporation rates and also on the salt chosen. The same crystallization condition yielded different crystal forms in microbatch and hanging-drop methods. For instance, in the presence of 0.2 *M* ammonium acetate as the salt, the hanging-drop method always yielded form 2 crystals, while microbatch method gave form 1 crystals (Table 2). Form 1 crystals only appeared using the microbatch method and form 3 crystals appeared only in hanging drops, while form 2 crystals were obtained in both. Form 1 crystals were obtained only in the presence of ammonium and potassium acetate in the microbatch method, while form 3 required sodium acetate instead in the hanging-drop setup. Both form 2 and form 3 crystals were observed in hanging-drop trials with sodium acetate. However, the ratio of precipitant to protein concentration and the volume of the well solution had an effect on the crystal size but not on the unit-cell parameter. The inclusion of additives ($SrCl_2$ and LiCl) also resulted in a change in the *c* axis, with values intermediate between those of form 1, form 2 and form 3. The crystallization conditions of the three crystal forms for which complete data sets were collected and used for further analysis are shown in bold in Table 2.

Table 2
Crystallization conditions.

The crystal structures discussed in this paper were obtained using the conditions shown in bold.

Salt	Crystallization method	Crystal form
Potassium acetate	Microbatch	Form 1
Ammonium acetate	**Microbatch**	**Form 1**
Ammonium acetate	**Hanging drop**	**Form 2**
Sodium acetate	Microbatch	Form 2
Lithum acetate	Microbatch	Form 2
Magnesium acetate	Microbatch	Form 2
Sodium acetate	**Hanging drop**	Form 2 and **form 3**

3.2. Structure solution of PfFabZ

The molecular-replacement program *Phaser* yielded clear solutions for form 2 and form 3 data, with *Z* scores of 29.55 and 28.50, and LLG values of 1256.67 and 743.52, respectively.

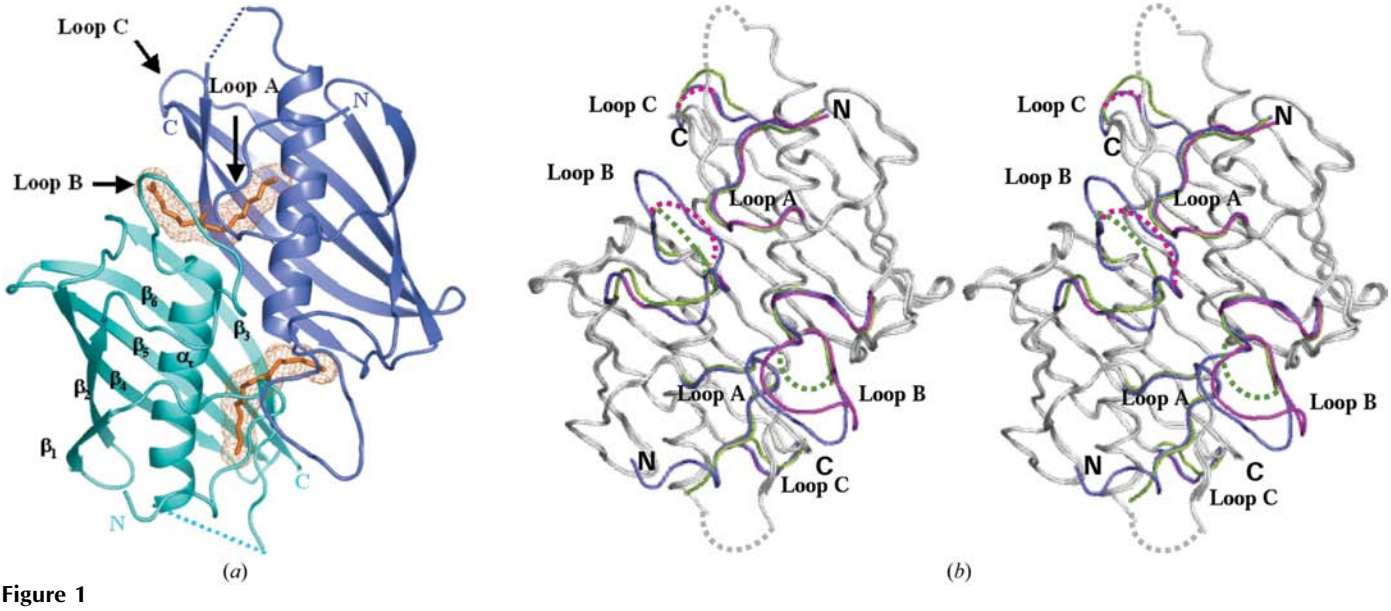

Figure 1
(*a*) Dimer of PfFabZ showing the two active-site tunnels. Subunits *A* and *B* of form 1 are shown in blue and cyan, respectively. The inhibitor 3-decenoyl-NAC modelled into the two active sites of d-PfFabZ is shown in mesh representation to highlight the tunnels. The broken lines represent disordered loops. (*b*) Stereoview of the superposition of the three forms of d-PfFabZ. The conformational differences in loops *A*, *B* and *C* are highlighted in blue (form 1), magenta (form 2) and green (form 3). The figures were generated using *PyMOL* (DeLano, 2002).

Iterative rounds of refinement using *CNS* and model building using the graphics program *Coot* followed by picking of solvent molecules yielded final R factors of 25.8 and 24.2% and $R_{\rm free}$ factors of 28.6 and 29.1%, respectively. Refinement

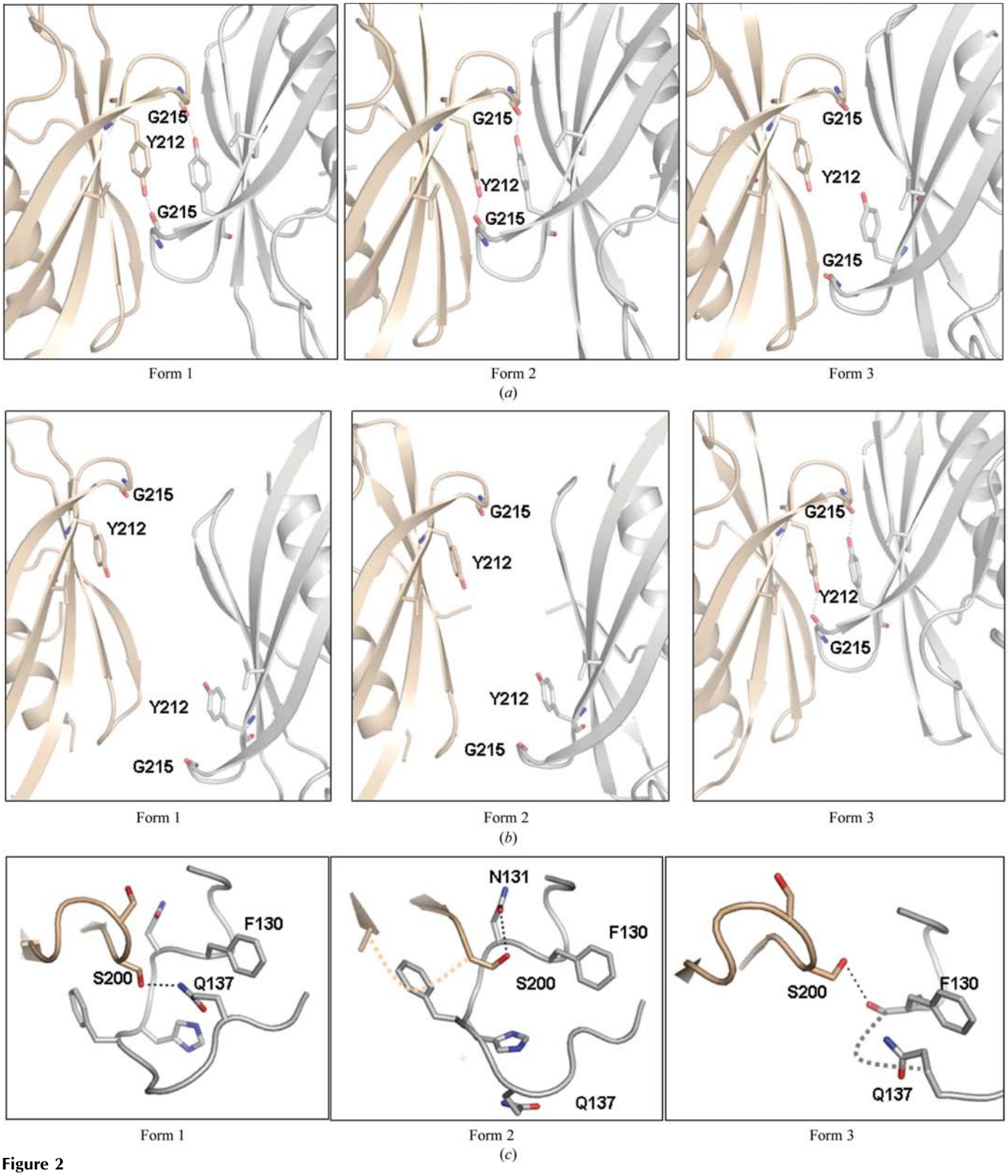

Figure 2
Packing differences observed at (*a*) Tyr212 of subunit *A* in the three crystal forms, looking down the *c* axis, and (*b*) Tyr212 of subunit *B* in the three crystal forms, looking down the *b* axis. (*c*) Interactions of loop *C* with loop *B* of a symmetry-related molecule. In crystal forms 2 and 3, loops *C* and *B*, respectively, are disordered. Hydrogen bonds are shown as black dotted lines and missing loops are shown as dotted lines in the corresponding colour. The reference molecule is shown in wheat and the symmetry-related molecule is shown in grey.

Table 3
Comparison of the three crystal forms of d-PfFabZ.

'—' indicates loops with missing residues.

	B factor (Å^2)						
	Loop *A*		Loop *B*		Loop *C*		
	Subunit *A*	Subunit *B*	Subunit *A*	Subunit *B*	Subunit *A*	Subunit *B*	Average *B* factor (Å^2)
Form 1	80	56	48	75	52	70	44
Form 2	120	92	84	—	—	105	60
Form 3	90	95	—	—	80	94	67

statistics are given in Table 1. *PROCHECK* analysis showed that the models contain 80.0 and 80.2% of residues in the most favoured region, 18.5 and 17.8% of residues in the allowed region and 1.5 and 2.0% of residues in generously allowed regions of the Ramachandran plot, respectively.

3.3. Overall features of PfFabZ structure

Each monomer of PfFabZ has a hot-dog fold similar to that of FabA from *Escherichia coli* (Leesong *et al.*, 1996) and FabZ from *Pseudomonas aureginosa* (PaFabZ; Kimber *et al.*, 2004). The hot-dog fold (Dillon & Bateman, 2004) consists of a six-stranded β-sheet wrapped around a central long α-helix. A dimer of hot dogs is formed by the association of the β-sheets to form a continuous 12-stranded β-sheet with the central helices running antiparallel to each other. The dimerization of PfFabZ results in the formation of two active-site tunnels at the dimer interface (Fig. 1*a*). Residues from the central helix, the N-terminal loop, loop *A* (Glu94–Leu103), the β-strand at the dimer interface (β3) from one subunit, loop *B* (Ser124–Met140) and other small regions from the other subunit line the active-site tunnel. The catalytic residues His133 and Glu147 are situated on loop *B* and the central helix, respectively. PfFabZ has an insertion of two serine residues (Ser200-Ser201) in the loop connecting β-strands β4 and β5 (loop *C*, Ser200–Gly203) which are absent in its bacterial counterparts. The loops *A*, *B* and *C* play an important role in determining the crystal packing and hence in determining the length of the *c* axis in the three crystal forms of d-PfFabZ.

3.4. Crystal structures of form 2 and form 3 of d-PfFabZ

Each subunit of the mature enzyme comprises 144 residues (Ile87–Lys230). For subunit *A*, 133, 125 and 122 residues are visible in the electron-density maps for the form 1, form 2 and form 3 crystals, respectively, whereas for subunit *B* the numbers of visible residues are 134, 123 and 122, respectively. Residues Asp161–Asn165, which belong to the loop connecting the central helix and β3, are not visible in the electron-density maps in both of the subunits of the form 2 and form 3 structures. These residues were absent in form 1 of d-PfFabZ as well as in PaFabZ. The dimers of form 2 and form 3 superpose with the dimer of form 1 with an r.m.s.d. of 0.28 and 0.59 Å, respectively, considering all atoms. The overall structures of the three forms of PfFabZ are identical; however, there are differences located in loops *A*, *B* and *C* (Fig. 1*b*). All three loops are well ordered in form 1. Although loop *A* had a high *B* factor, the electron density was sufficiently clear to trace the loop. In form 2 and form 3 crystals, the high temperature factors of loop *A* indicate its flexibility, while some of the residues from loops *B* and *C* could not be modelled. The differences are tabulated in Table 3.

3.5. Packing analysis

Crystal-packing analysis shows that although the dimers are identical, they differ in the manner they are arranged in the unit cell (Fig. 2). The dimers of form 2 and form 3 are oriented at 1.6 and 16.0°, respectively, with respect to form 1, the angle being measured between the twofold axis that relates the two monomers in each dimer. A clear view of the differences in crystal packing can be observed at the crystallographic twofold axis that relates Tyr212 to the same residue from a symmetry-related molecule. The hydroxyl group of Tyr212 forms a hydrogen bond with the carbonyl O atom of Gly215 between the *A* subunits of symmetry-related molecules in form 1 and form 2 (Fig. 2*a*). In form 3, this interaction is missing as the dimer is rotated by 16° when compared with form 1. In Fig. 2(*b*), looking down the *b* axis, it can be observed that the distance between Tyr212 OH of the *B* subunit and the same residue of the symmetry-related molecule increases with the length of the *c* axis. In addition, the aromatic rings of the tyrosines are involved in good stacking interactions in the *A* subunit of form 1 and form 2 and the *B* subunit of form 3. Similar interactions are missing in the *A* subunit of form 3 and the *B* subunit of form 1 and form 2 as the distance between the tyrosines increases owing to differences in crystal packing. Thus, the difference in the orientation of the molecules in the three crystal forms is strongly correlated to the length of the *c* axis.[1]

As can be observed from Table 3, in form 3, with the shortest *c* axis, only loop *C* is ordered and the residues Asn131–Lys137 from loop *B* are not seen in electron density. In the case of form 2, with an intermediate *c* axis, loop *B* from subunit *A* and loop *C* from subunit *B* are ordered and residues His133–Lys137 from the *B* subunit and Ser201–Ile204 from the *A* subunit are not seen in the electron density. This observation indicates that loops *B* and *C* of the symmetry-related molecules compete for the space available. The OG atom of Ser200 in loop *C* appears to play a role in holding the two loops *B* and *C* in place between the symmetry-related molecules. As shown in Fig. 2(*c*), this atom makes hydrogen bonds to different atoms of loop *B* (Gln137 OD1 in form 1, Asn131 OD1 in form 2 and Phe130 N in form 3) as the conformation of loop *B* changes in the various forms. To further confirm this observation that form 2 and form 3 cannot accommodate all ordered loops, the form 1 dimer, in which all the residues of the three loops are seen in electron density, was superposed onto the other two dimers and the interactions with symmetry-related molecules were examined in the

[1] Supplementary material, including packing diagrams, has been deposited in the IUCr electronic archive (Reference: BE5078). Services for accessing this material are described at the back of the journal.

respective unit cells. Severe short contacts of distance less than 1 Å between the residues of loops *B* and *C* confirm that the orientation differences in packing are indeed a consequence of the competition between loops *B* and *C* of symmetry-related molecules.

As can be observed from Table 3, the average *B* factor of form 1 is the lowest of the three crystal forms. In the case of form 2 and form 3 crystals, although the packing becomes tighter, the molecules do not have enough space between them to be completely ordered, which is reflected in their high average *B* factors, indicating that tighter packing may not always result in more ordered molecules. There exists an optimum volume of the unit cell that is needed to pack the completely ordered molecule, which in this case is the form 1 crystal. Crystallization results clearly show that crystals of form 2 and form 3 of good diffraction quality are mostly obtained by the hanging-drop vapour-diffusion method, in which the evaporation rate is high. On the other hand, form 1 crystals could only be obtained using the microbatch method with a low evaporation rate and sufficient time for the loops to stabilize. This is consistent with our observation from dynamic light-scattering experiments that the time required for PfFabZ to form stable dimers at low pH is around 8 h (Swarnamukhi *et al.*, 2006). Our analysis clearly indicates that the differences in the evaporation rates in the crystallization methods adopted and the crystallization conditions can lead to significant differences in packing. In a recent review, Heras & Martin (2005) note that the diffraction quality of a number of protein crystals was improved significantly by post-crystallization treatments such as dehydration that make the crystals more ordered owing to changes in crystal packing.

3.6. Conformational changes at low pH

In addition to our recently reported crystal structure of d-PfFabZ (Swarnamukhi *et al.*, 2006), another crystal structure of PfFabZ in a hexameric state has been reported (Kostrewa *et al.*, 2005). When the crystal structures of the two forms were compared, the conformations of the two active-site loops *A* and *B* were observed to differ between the structures, the major difference between these two oligomeric states being the pH at which they were crystallized. The dimeric state was crystallized at low pH (4.5) and the hexameric form was crystallized at higher pH (6.0). Our dynamic light-scattering and gel-filtration studies clearly showed that PfFabZ exists as a dimer at low pH and as a hexamer at high pH in solution (Swarnamukhi *et al.*, 2006). Interconversion of the oligomeric states from hexamers to dimers and *vice versa* is possible by changing the pH. The conformational change in the active-site loops is initiated by the repulsion between two histidines at the active site followed by two *cis–trans* peptide flips at low pH. Thus, crystallization at low pH induces conformational changes in the protein.

Three crystal forms of d-PfFabZ with a variable *c* axis in the *I*222 unit cell were obtained at low pH. The crystal structures of the three forms are identical except for differences in loops *A*, *B* and *C*. Crystal-packing analysis has shown that in form 2 and form 3 steric hindrance leads to different conformations of loops *B* and *C*. Previous studies show pH-induced oligomeric shifts in PfFabZ. At low pH, the active-site loops *A* and *B* undergo large conformational changes which lead to the readjustment of the molecules that are close together in the crystalline lattice, thus leading to the packing differences. These effects are enhanced by variations in the experimental conditions of the crystallization trials.

4. Conclusion

The crystals of dimeric PfFabZ show non-isomorphism, with varying lengths of the *c* axis in the *I*222 cell. Small variations in crystallization conditions lead to large differences in crystal packing and hence in the length of the *c* axis. Crystal-packing analysis showed that loops *B* and *C* of symmetry-related molecules compete for space in the crystal forms with smaller *c* axes. The pH-induced conformational changes in loops *A* and *B* combined with the differences in the evaporation rates and small variations in the contents of the crystallization cocktail might be responsible for the observed non-isomorphism.

Intensity data were collected at the X-ray Facility for Structural Biology supported by the Department of Science and Technology (DST) and the Department of Biotechnology (DBT). Computations were carried out at the Bioinformatics Centre and Graphics Facility (both supported by DBT) and the Supercomputer Education and Research Centre at the Institute. This work was supported by a grant from DBT to KS and NS.

References

Brock, D. J., Kass, L. R. & Bloch, K. (1967). *J. Biol. Chem.* **242**, 4432–4440.
Brodersen, D. E., Clemons, W. M. Jr, Carter, A. P., Wimberly, B. T. & Ramakrishnan, V. (2003). *Acta Cryst.* D**59**, 2044–2050.
Brünger, A. T., Adams, P. D., Clore, G. M., DeLano, W. L., Gros, P., Grosse-Kunstleve, R. W., Jiang, J.-S., Kuszewski, J., Nilges, M., Pannu, N. S., Read, R. J., Rice, L. M., Simonson, T. & Warren, G. L. (1998). *Acta Cryst.* D**54**, 905–921.
Cohen, G. H. (1997). *J. Appl. Cryst.* **30**, 1160–1161.
Collaborative Computational Project, Number 4 (1994). *Acta Cryst.* D**50**, 760–763.
Dauter, Z., Botos, I., La Ronde-Le Blanc, N. & Wlodawer, A. (2005). *Acta Cryst.* D**61**, 967–975.
DeLano, W. L. (2002). *The PyMOL Molecular Graphics System.* DeLano Scientific, San Carlos, USA http://www.pymol.org.
Dillon, S. C. & Bateman, A. (2004). *BMC Bioinformatics*, **5**, 109.
Emsley, P. & Cowtan, K. (2004). *Acta Cryst.* D**60**, 2126–2132.
Heath, R. J. & Rock, C. O. (1996). *J. Biol. Chem.* **271**, 27795–27801.
Heras, B. & Martin, J. L. (2005). *Acta Cryst.* D**61**, 1173–1180.
Kimber, M. S., Martin, F., Lu, Y., Houston, S., Vedadi, M., Dharamsi, A., Fiebig, K. M., Schmid, M. & Rock, C. O. (2004). *J. Biol. Chem.* **279**, 52593–52602.
Kostrewa, D., Winkler, F. K., Folkers, G., Scapozza, L. & Perozzo, R. (2005). *Protein Sci.* **14**, 1570–1580.

Laskowski, R. A., MacArthur, M. W., Moss, D. S. & Thornton, J. M. (1993). *J. Appl. Cryst.* **26**, 283–291.
Leesong, M., Henderson, B. S., Gillig, J. R., Schwab, J. M. & Smith, J. L. (1996). *Structure*, **4**, 253–264.
Mukhi, P. L. S., Sharma, S. K., Kapoor, M., Surolia, N., Surolia, A. & Suguna, K. (2004). *Acta Cryst.* D**60**, 120–121.
Otwinowski, Z. & Minor, W. (1997). *Methods Enzymol.* **267**, 307–326.
Raetz, C. R. H. (1990). *Annu. Rev. Biochem.* **59**, 129–170.
Randal, M. & Kossiakoff, A. A. (2000). *Acta Cryst.* D**56**, 14–24.
Redinbo, M. R., Stewart, L., Champoux, J. J. & Hol, W. G. J. (1999). *J. Mol. Biol.* **292**, 685–696.
Rock, C. O. & Cronan, J. E. (1996). *Biochim. Biophys. Acta*, **1302**, 1–16.
Sharma, S. K., Kapoor, M., Ramya, T. N. C., Kumar, S., Kumar, G., Modak, R., Sharma, S., Surolia, N. & Suroia, A. (2003). *J. Biol. Chem.* **278**, 45661–45671.
Storoni, L. C., McCoy, A. J. & Read, R. J. (2004). *Acta Cryst.* D**60**, 432–438.
Swarnamukhi, P. L., Sharma, S. K., Bajaj, P., Surolia, N., Surolia, A. & Suguna, K. (2006). *FEBS Lett.* **580**, 2653–2660.
Verschueren, K. H. G., Tyrrell, R., Murshudov, G. N., Dodson, E. & Wilkinson, A. J. (1999). *Acta Cryst.* D**55**, 369–378.